

Testing coalescence and statistical-thermal production scenarios for (anti-)(hyper-)nuclei at LHC energies with recent and future Run 3 and 4 data

F. Bellini and A. Kalweit

26th of February 2018

(Anti-)(hyper-)nuclei are unique probes of the medium created in proton-proton, proton-Pb, and Pb-Pb collisions at LHC energies. At LHC energies, their production is typically discussed within the framework of coalescence and thermal-statistical production models. While it is often argued that both approaches are not distinguishable, we present a detailed study of both theories which reveals largely different predictions between the two approach for the production of ^3He and hyper-tritons. Confronting our results with recent ALICE measurements, the coalescence approach is found to provide a correct description of the data only in small systems such as pp collisions, while it fails for central Pb-Pb collisions. The thermal-statistical model on the other hand is in agreement with results in central Pb-Pb collisions even though such fragile objects should be destroyed in hadronic interactions after the chemical freeze-out of the system. Our finding thus indicate the existence of a novel production mechanism for these objects.

Contents

1	Introduction	2
2	Coalescence approach	3
2.1	Simple coalescence	3
2.2	Full coalescence	3
2.3	Source volume	5
3	Statistical-thermal approach and blast-wave	6
4	Comparison with experimental data	6
4.1	(Anti-)nuclei with $A = 2, 3, 4$	6
4.2	(Anti-)hyper-nuclei	6
5	Projections for the LHC Run 3 and 4	6
6	Summary and conclusions	6

1 Introduction

The formation of light anti- and hyper- nuclei in highly energetic proton-proton, proton-nucleus and nucleus-nucleus collisions provides unique observables for the study of the system created in these collisions. In this context, nuclei and hyper-nuclei are special objects with respect to non-composite hadrons, because their size is comparable to a fraction or the whole system created in the collision []. The relevant properties of the objects under study are summarised in Table 1. As quantum-mechanical objects, their size is typically defined as the rms of their wave function, which ranges from **xx fm for the ^3He up to yy fm for the hyper-triton**. Halo nuclei as ^6He would be ideal for such studies, but they remain out of the experimental reach in high-energy experiments in the near future.

Surprisingly, thermal-statistical models have been successful at describing not only light-flavour particle production, but also that of light (anti-)(hyper-)nuclei across a wide range of energies in nucleus-nucleus collisions [1, 2]. In this approach, particles are produced from a fireball in thermal and kinetic equilibrium with temperatures of the order of $T_{chem} = 156$ MeV (near the temperature at the QCD phase transition boundary, as predicted by lattice QCD calculations [3]). Particle abundances are fixed at chemical freeze-out, when inelastic collisions cease. Further elastic and pseudo-elastic collisions occur among the components of the expanding fireball, that can affect the spectral shapes and the measurable yields of short-lived (strongly decaying) hadronic resonances. Once the particle density of the system is so low that the mean free path for elastic collisions is larger than the size of the system, the fireball freezes-out kinetically. This is seen to occur when the system has reached temperatures of the order of $T_{kin} \approx 90$ MeV. In such a dense and hot environment, composite objects with binding energies that are small with respect to the temperature of the system, appear as “fragile” objects. For instance, the binding energy of the deuteron is $E_{B,d} = 2.2$ MeV $\ll T_{chem}, T_{kin}$. As a matter of fact, the cross-section for pion-induced deuteron breakup is significantly larger than the typical (pseudo)-elastic cross-sections for the re-scattering of hadronic resonance decay products (check statement) [4, 5, 6]. Similarly, the elastic cross-section which drives the deuteron spectra to kinetic equilibration in central heavy-ion collisions [7] is **smaller than the breakup cross-section** [6]. Based on this, the deuterons produced at chemical freeze-out would be expected not to survive the hadronic phase of the medium expansion, yet their production is measured to be consistent to the predictions from statistical-thermal models and they develop also a non-zero elliptic flow which is consistent with a common radial expansion together with the non-composite hadrons [7]. **Do similar estimates as Karel in Frascati**. In addition, it was recently shown that the assumption of realistic eigenvolumina for light nuclei would lead to instabilities of the statistical/thermal model predictions [8]. Several solutions have been proposed to solve this “light (anti-)nuclei puzzle”: (a.) a sudden freeze-out at the QGP-hadron phase boundary, (b.) the thermal production of these objects as compact quark bags [1], and (c.) the coincidence of coalescence mechanism with that of thermal production [9]. Data from rescattering of short-lived hadronic resonances indicate that the system undergoes a long-lasting hadronic phase before decoupling [10], thus strongly disfavouring hypothesis (a.). While hypothesis (b.) cannot presently be tested beyond the agreement of measured (anti-)nuclei production yields with statistical-thermal model predictions, hypothesis (c.) is scrutinised in the present work.

To this purpose, we compare to models the existing data from the Large Hadron Collider. For the first time, these data allow for the systematic study of the light (anti-)(hyper-)nuclei production as a function of the system and object size. In the nucleon-coalescence approach, nuclei are formed at kinetic freeze-out by coalescence of nucleons that are nearby in space and have similar velocities. The coalescence model is reviewed in Section 2, starting from its simplest form (uncorrelated nucleon emission from a point-like source) to the full space-time evolution picture as discussed in [9]. In section 3, a blast-wave parameterisation for particle transverse momentum spectra in combination with predictions from the statistical-thermal model for the yields is used as an alternative approach. The direct comparison of the two approaches and the comparison with data are discussed in section 4. We find that a systematic study of the coalescence parameter B_A provides an important discrimination power between the two approaches. A comparison of the production rates of nuclei with similar mass but very different internal structure has already been suggested for the case of ^4He and ^4Li [11]. However, as the ^4Li is not stable with respect to strong decay, its measurement is experimentally very challenging and probably less constraining than the comparison with hyper-nuclei proposed here. In

section 5 we propose that B_A is systematically measured in all collision systems by exploiting the large statistics sample that will be available with the LHC Run 3 and 4, in order to rule out or support the aforementioned scenarios. As a matter of fact, the upcoming years of LHC data taking provide a unique opportunity to for the final understanding of (anti-)(hyper-)nuclei production. Setting a final word on the production mechanisms is not only in the interest of the heavy-ion community, but has a broader application in astrophysics and dark-matter searches, by representing an essential input for the measurement of (anti-)nuclei in space with ongoing [12] and future [?, 13] experiments. In addition to this, the study of light(anti-)nuclei might serve as a baseline for understanding the debated nature of exotic states such as the X(3872), that has been interpreted as tetraquark state or hadronic molecule [14, 15].

2 Coalescence approach

2.1 Simple coalescence

In simple coalescence, nucleons produced in the collision coalesce into nuclei if they are close in space and have similar velocities [16, 17]. For a nucleus with mass number $A = Z + N$, the coalescence probability is typically quantified in terms of the coalescence parameter B_A , which is defined as

$$E_A \frac{d^3 N_A}{dp_A^3} = B_A \left(E_p \frac{d^3 N_p}{dp_p^3} \right)^Z \left(E_n \frac{d^3 N_n}{dp_n^3} \right)^N \Big|_{\vec{p}_p = \vec{p}_n = \frac{\vec{p}_A}{A}} , \quad (1)$$

where $p_{p,n}$ are the momenta of the proton and neutron and $E_{p,n}$ their energy. Since at LHC energies the number of produced protons and neutrons at midrapidity is expected to be equal, the equation simplifies to

$$E_A \frac{d^3 N_A}{dp_A^3} = B_A \left(E_p \frac{d^3 N_p}{dp_p^3} \right)^A \Big|_{\vec{p}_p = \frac{\vec{p}_A}{A}} . \quad (2)$$

Moreover, the LHC is particularly suited for the production of anti-nuclei, since the number of baryons and anti-baryons is essentially equal at midrapidity [18]. In a simple coalescence approach, the coalescence parameter is expected to be independent of p_T and of the object size with respect to the volume of particle emission (hereafter referred to as “source volume” or “source size”). In this naive expectation, the number of nuclei produced by coalescence increases with increasing number of nucleons produced in the collision. If the nucleon number increases with the event multiplicity, so does the number of (anti-)nuclei. While this picture is found to be approximately valid in pp and p–Pb collisions [19, 20], it breaks down in Pb–Pb collisions, that exhibit a strong decrease of B_A with the centrality of the collision [21]. In addition, the elliptic flow of deuteron cannot be explained by simple coalescence [22].

Mass number	Nucleus	Composition	B_E (MeV)	rms radius of wavefunction (fm)	Refs.
A = 2	d	pn	2.2	3.2	
A = 3	^3H	pnn			
	^3He	ppn			
A = 4	$^3_\Lambda\text{H}$	p Λ n			
	^4He	ppnn			
	$^4_\Lambda\text{H}$	p Λ nn			
	$^4_{\Lambda\Lambda}\text{H}$	p $\Lambda\Lambda$ n			
	$^4_\Lambda\text{He}$	pp Λ n			

Table 1: Properties of nuclei and hyper-nuclei. B_E is the binding energy per nucleon in MeV and the radius is given in terms of the rms radius of the wavefunction. References are given in the last column.

2.2 Full coalescence

In contrast to the simple approach described in the previous section, a more advanced coalescence model takes into account the size of the particle emission source, as the coalescence probability naturally decreases for two nucleons with similar momenta that are produced far apart in configuration space. While there are several approaches to address this effect [?], we rely in our study on the formalism proposed in [9]. **Consider mentioning the approximations done by Uli in his paper, if there is time and how Uli's paper relates to the Wigner formalism.** In this approach, the quantum mechanical nature of the coalescence products is explicitly accounted for by means of an average quantum mechanical correction factor, $\langle C_A \rangle$. In the case of the deuteron, the quantum mechanical correction factor $\langle C_d \rangle$ has been approximated as

$$\langle C_d \rangle \approx \frac{1}{\left[1 + \left(\frac{r_d}{2R_\perp(m_T)}\right)^2\right] \sqrt{1 + \left(\frac{r_d}{2R_\parallel(m_T)}\right)^2}} \quad (3)$$

where r_d is the radius of the deuteron, R_\perp and R_\parallel are the lengths of homogeneity of the coalescence volume and m_T is the transverse mass of the coalescing nucleons. The size of the nucleus enters in the determination of the coalescence parameter B_2 via the quantum-mechanical correction factor $\langle C_d \rangle$, as well as the homogeneity volume $R_\perp^2 R_\parallel$, according to the relation

$$B_2 = \frac{3\pi^{3/2} \langle C_d \rangle}{2m_T R_\perp^2(m_T) R_\parallel(m_T)} \quad (4)$$

which is the main result of [9]. It is interesting to note that the coalescence parameter decreases with increasing volume, as expected. In addition to this, the quantum mechanical correction factor introduces a length scale defined by the deuteron size relative to the source size in the calculation of B_2 , which reflects the coalescence probability. If we assume that $R_\perp \approx R_\parallel \approx R$, Eqs. 3 and 4 simplify to

$$\langle C_d \rangle \approx \left[1 + \left(\frac{r_d}{2R(m_T)}\right)^2\right]^{-3/2} \quad (5)$$

and

$$B_2 = \frac{3\pi^{3/2} \langle C_d \rangle}{2m_T R^3(m_T)}. \quad (6)$$

Figure 1 shows the source radius (R) dependence of the quantum-mechanical correction factor (on the left) and the coalescence parameter B_2 (on the right), calculated assuming (a.) a point-like nucleus, (b.) $r_d = 0.3$ fm as currently assumed in thermal model calculations [23], (c.) the current estimate of the rms radius of the deuteron $r_d = 3.2$ fm [24], (d.) a larger, unrealistic value of $r_d = 10$ fm. As can be seen in Fig. 1, the quantum-mechanical correction factor leads to a significant suppression in the production of those objects whose radius is large compared to that of the source.

Following the approach and discussion presented in [25], Eq. 3 may be generalised as

$$\langle C_A \rangle = \prod_{i=1,2,3} \left(1 + \frac{r^2}{4R_i^2}\right)^{-\frac{1}{2}(A-1)} \quad (7)$$

for mass number A and the radii R_i which describe the volume of the emitting source. Similarly, the coalescence parameter B_A for a nucleus with mass number A and spin J_A is generalised in [9] as

$$B_A = \frac{2J_A + 1}{2^A} \frac{1}{\sqrt{A}} \langle C_A \rangle \left(\frac{(2\pi)^{3/2}}{m_T \prod_{i=1,2,3} R_i} \right)^{A-1}. \quad (8)$$

In particular, for the case of ${}^3\text{He}$ with $A = 3$ and $J = 1/2$, Eq. 8 becomes Eq. 9 presented in [25]:

$$B_3 = \frac{(2\pi)^3}{4\sqrt{3}} \langle C_3 \rangle (m_T \prod_{i=1,2,3} R_i)^{-2} \quad (9)$$

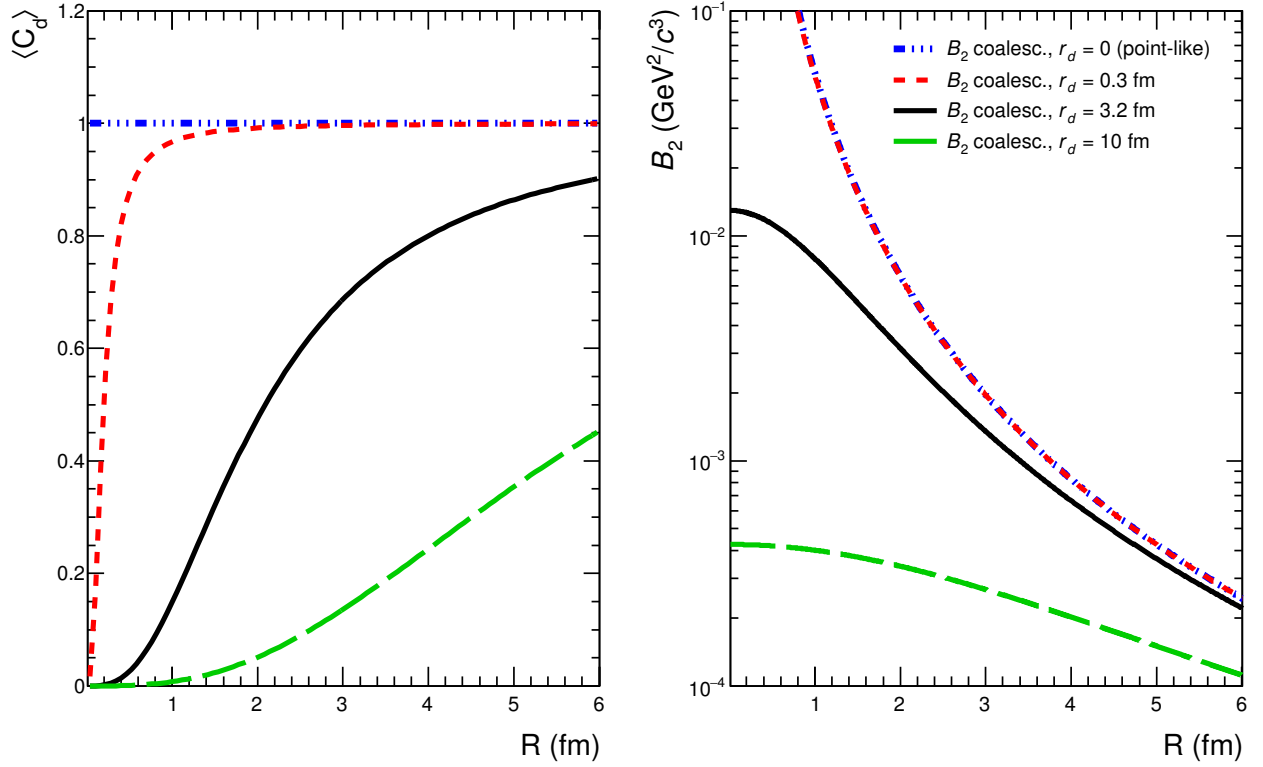


Figure 1: The quantum mechanical correction factor $\langle C_d \rangle$ (left panel, see Eq. 5) and the coalescence parameter B_2 for deuteron (right panel, see Eq. 6) as a function of the radius of the source, R , calculated assuming a radius of the deuteron $r_d = 0, 0.3, 3.2$ and 10 fm.

where

$$\langle C_3 \rangle \approx \prod_{i=1,2,3} \left(1 + \frac{r_3^2}{4R_i^2} \right)^{-1}. \quad (10)$$

2.3 Source volume

As in [9], we identify the source volume as the effective sub-volume of the whole system which is governed by the homogeneity length of the interacting nucleons. In addition, the same authors claim that this volume is experimentally accessible with Hanbury-Brown-Twiss (HBT) interferometry. Experimentally, the size of the effective volume can be controlled by selecting different collision geometries, i.e. different centrality classes [26]. In heavy-ion collisions the HBT radii are known to scale with the cubic root of the average charged particle multiplicity density $\langle dN_{\text{ch}}/d\eta \rangle^{1/3}$ [27], and to depend on the pair average transverse momentum $\langle k_T \rangle$ [28]. In the following, we make the simplifying assumption that the scaling with $\langle dN_{\text{ch}}/d\eta \rangle^{1/3}$ holds across collision systems, which is approximately fulfilled in data [29]. In contrast to [25], we therefore do not explicitly use the measured HBT radii in our study, but we derive the radii from the measured $\langle dN_{\text{ch}}/d\eta \rangle$ according to the following relation:

$$R = a + b \langle dN_{\text{ch}}/d\eta \rangle^{1/3} \quad (11)$$

The $a = 0.178$ and $b = 0.367$ coefficients have been determined empirically by interpolating linearly between the value of 0.85 fm and 4.5 fm. These values are consistent with the radius from kaon femtoscopy for $m_T \approx 1$ GeV/ c in low-multiplicity pp collisions [30] and the radius from pion femtoscopy in high-multiplicity Pb-Pb collisions at the highest available $k_T \approx 0.8$ GeV/ c [27]. The highest k_T bin was chosen as it corresponds in m_T to the lowest transverse momentum per nucleon ($p_T/A \approx 0.8$ GeV/ c) accessible by ALICE for the measurement of nuclei production. Ideally, one would use the

158 proton femtoscopic radii for such study, but given that these measurements are not available in all
159 systems, we assume that m_T -scaling holds for HBT radii [31].
160 - mention that the parameterisation we propose is found to describe the deuteron data - mention
161 we assume the three radii are the same, see line 127 - plot our parameterisation vs the HBT results:
162 take figure 9 from the femto p-Pb paper but do it at high kt and plot one radii which is the geometric
163 average of the three.

Figure 2: Parameterisation of the dependence of the source radius on multiplicity assumed in this paper, compared to HBT data.

164 - excess binding energy needs to be released to the system to make coalescence work

165 3 Statistical-thermal approach and blast-wave

166 -

167 4 Comparison with experimental data

168 4.1 (Anti-)nuclei with $A = 2, 3, 4$

169 4.2 (Anti-)hyper-nuclei

170 - cite Che Ming Ko [32]

171 5 Projections for the LHC Run 3 and 4

172 6 Summary and conclusions

173 We conclude that (c.) appears unlikely, thus leaving (b.) as a viable option, at least with our present
174 knowledge of the hypertriton size.

175 Acknowledgements

176 The authors would like to thank themselves for the auto-critics.

177 References

- 178 [1] A. Andronic, P. Braun-Munzinger, K. Redlich, and J. Stachel, “Decoding the phase structure of
179 QCD via particle production at high energy,” [arXiv:1710.09425](https://arxiv.org/abs/1710.09425) [nucl-th].
- 180 [2] A. Andronic, P. Braun-Munzinger, J. Stachel, and H. Stäcker, “Production of light nuclei,
181 hypernuclei and their antiparticles in relativistic nuclear collisions,” *Physics Letters B* **697** no. 3,
182 (2011) 203 – 207. <http://www.sciencedirect.com/science/article/pii/S0370269311001006>.
- 183 [3] **HotQCD** Collaboration, A. Bazavov *et al.*, “Equation of state in (2+1)-flavor QCD,” *Phys.*
184 *Rev. D* **90** (2014) 094503, [arXiv:1407.6387](https://arxiv.org/abs/1407.6387) [hep-lat].
- 185 [4] H. Garcilazo, “PION DEUTERON BREAKUP IN THE REGION OF THE (3,3)
186 RESONANCE,” *Phys. Rev. Lett.* **48** (1982) 577–580.
- 187 [5] S. A. Bass *et al.*, “Microscopic models for ultrarelativistic heavy ion collisions,” *Prog. Part. Nucl.*
188 *Phys.* **41** (1998) 255–369, [arXiv:nuc1-th/9803035](https://arxiv.org/abs/nuc1-th/9803035) [nucl-th]. [Prog. Part. Nucl.
189 Phys.41,225(1998)].

- [6] J. Schukraft, “QM2017: Status and Key open Questions in Ultra-Relativistic Heavy-Ion Physics,” *Nucl. Phys.* **A967** (2017) 1–10, [arXiv:1705.02646 \[hep-ex\]](#).
- [7] **ALICE** Collaboration, S. Acharya *et al.*, “Measurement of deuteron spectra and elliptic flow in Pb-Pb collisions at $\sqrt{s_{NN}} = 2.76$ TeV at the LHC,” *Eur. Phys. J.* **C77** no. 10, (2017) 658, [arXiv:1707.07304 \[nucl-ex\]](#).
- [8] V. Vovchenko and H. Stoecker, “Analysis of hadron yield data within hadron resonance gas model with multi-component eigenvolume corrections,” *J. Phys. Conf. Ser.* **779** no. 1, (2017) 012078, [arXiv:1610.02346 \[nucl-th\]](#).
- [9] R. Scheibl and U. W. Heinz, “Coalescence and flow in ultrarelativistic heavy ion collisions,” *Phys. Rev.* **C59** (1999) 1585–1602, [arXiv:nucl-th/9809092 \[nucl-th\]](#).
- [10] **ALICE** Collaboration, B. B. Abelev *et al.*, “ $K^*(892)^0$ and $\Lambda(1020)$ production in Pb-Pb collisions at $\sqrt{s_{NN}} = 2.76$ TeV,” *Phys. Rev.* **C91** (2015) 024609, [arXiv:1404.0495 \[nucl-ex\]](#).
- [11] S. Bazak and S. Mrowczynski, “ ^4He vs. ^4Li and production of light nuclei in relativistic heavy-ion collisions,” [arXiv:1802.08212 \[nucl-th\]](#).
- [12] **AMS** Collaboration, J. Alcaraz *et al.*, “Search for anti-helium in cosmic rays,” *Phys. Lett.* **B461** (1999) 387–396, [arXiv:hep-ex/0002048 \[hep-ex\]](#).
- [13] **GAPS** Collaboration, T. Aramaki, C. J. Hailey, S. E. Boggs, P. von Doetinchem, H. Fuke, S. I. Mognet, R. A. Ong, K. Perez, and J. Zweerink, “Antideuteron Sensitivity for the GAPS Experiment,” *Astropart. Phys.* **74** (2016) 6–13, [arXiv:1506.02513 \[astro-ph.HE\]](#).
- [14] A. Esposito, A. L. Guerrieri, L. Maiani, F. Piccinini, A. Pilloni, A. D. Polosa, and V. Riquer, “Observation of light nuclei at ALICE and the X(3872) conundrum,” *Phys. Rev.* **D92** no. 3, (2015) 034028, [arXiv:1508.00295 \[hep-ph\]](#).
- [15] **ExHIC** Collaboration, S. Cho *et al.*, “Exotic Hadrons from Heavy Ion Collisions,” *Prog. Part. Nucl. Phys.* **95** (2017) 279–322, [arXiv:1702.00486 \[nucl-th\]](#).
- [16] S. T. Butler and C. A. Pearson, “Deuterons from High-Energy Proton Bombardment of Matter,” *Phys. Rev.* **129** (1963) 836–842.
- [17] J. I. Kapusta, “Mechanisms for deuteron production in relativistic nuclear collisions,” *Phys. Rev.* **C21** (1980) 1301–1310.
- [18] **ALICE** Collaboration, E. Abbas *et al.*, “Mid-rapidity anti-baryon to baryon ratios in pp collisions at $\sqrt{s} = 0.9, 2.76$ and 7 TeV measured by ALICE,” *Eur. Phys. J.* **C73** (2013) 2496, [arXiv:1305.1562 \[nucl-ex\]](#).
- [19] **ALICE** Collaboration, S. Acharya *et al.*, “Production of deuterons, tritons, ^3He nuclei and their antinuclei in pp collisions at $\sqrt{s} = 0.9, 2.76$ and 7 TeV,” *Phys. Rev.* **C97** no. 2, (2018) 024615, [arXiv:1709.08522 \[nucl-ex\]](#).
- [20] **ALICE** Collaboration, S. Acharya *et al.*, “Multiplicity dependence of (anti-)nuclei production in p-Pb collisions at $\sqrt{s_{NN}} = 5.02$ TeV,” *To be published* **xx** (2018) yy, [arXiv:xxxx.xxxx \[nucl-ex\]](#).
- [21] **ALICE** Collaboration, J. Adam *et al.*, “Production of light nuclei and anti-nuclei in pp and Pb-Pb collisions at energies available at the CERN Large Hadron Collider,” *Phys. Rev.* **C93** no. 2, (2016) 024917, [arXiv:1506.08951 \[nucl-ex\]](#).
- [22] **ALICE** Collaboration, S. Acharya *et al.*, “Measurement of deuteron spectra and elliptic flow in Pb-Pb collisions at $\sqrt{s_{NN}} = 2.76$ TeV at the LHC,” *Eur. Phys. J.* **C77** no. 10, (2017) 658, [arXiv:1707.07304 \[nucl-ex\]](#).

- [23] A. Andronic, P. Braun-Munzinger, K. Redlich, and J. Stachel, “Hadron yields, the chemical freeze-out and the QCD phase diagram,” *J. Phys. Conf. Ser.* **779** no. 1, (2017) 012012, [arXiv:1611.01347 \[nucl-th\]](#).
- [24] P. J. Mohr, D. B. Newell, and B. N. Taylor, “CODATA Recommended Values of the Fundamental Physical Constants: 2014,” *Rev. Mod. Phys.* **88** no. 3, (2016) 035009, [arXiv:1507.07956 \[physics.atom-ph\]](#).
- [25] K. Blum, K. C. Y. Ng, R. Sato, and M. Takimoto, “Cosmic rays, antihelium, and an old navy spotlight,” *Phys. Rev.* **D96** no. 10, (2017) 103021, [arXiv:1704.05431 \[astro-ph.HE\]](#).
- [26] **ALICE** Collaboration, B. Abelev *et al.*, “Centrality determination of Pb-Pb collisions at $\sqrt{s_{NN}} = 2.76$ TeV with ALICE,” *Phys. Rev.* **C88** no. 4, (2013) 044909, [arXiv:1301.4361 \[nucl-ex\]](#).
- [27] **ALICE** Collaboration, J. Adam *et al.*, “Centrality dependence of pion freeze-out radii in Pb-Pb collisions at $\sqrt{s_{NN}} = 2.76$ TeV,” *Phys. Rev.* **C93** no. 2, (2016) 024905, [arXiv:1507.06842 \[nucl-ex\]](#).
- [28] **ALICE** Collaboration, K. Aamodt *et al.*, “Two-pion Bose-Einstein correlations in central Pb-Pb collisions at $\sqrt{s_{NN}} = 2.76$ TeV,” *Phys. Lett.* **B696** (2011) 328–337, [arXiv:1012.4035 \[nucl-ex\]](#).
- [29] **ALICE** Collaboration, J. Adam *et al.*, “Two-pion femtoscopy in p-Pb collisions at $\sqrt{s_{NN}} = 5.02$ TeV,” *Phys. Rev.* **C91** (2015) 034906, [arXiv:1502.00559 \[nucl-ex\]](#).
- [30] **ALICE** Collaboration, B. Abelev *et al.*, “Charged kaon femtoscopic correlations in *pp* collisions at $\sqrt{s} = 7$ TeV,” *Phys. Rev.* **D87** no. 5, (2013) 052016, [arXiv:1212.5958 \[hep-ex\]](#).
- [31] **ALICE** Collaboration, J. Adam *et al.*, “One-dimensional pion, kaon, and proton femtoscopy in Pb-Pb collisions at $\sqrt{s_{NN}} = 2.76$ TeV,” *Phys. Rev.* **C92** no. 5, (2015) 054908, [arXiv:1506.07884 \[nucl-ex\]](#).
- [32] Z. Zhang and C. M. Ko, “Hypertriton production in relativistic heavy ion collisions,” *Phys. Lett.* **B780** (2018) 191–195.